Reconstruction of objects above and below the objective focal plane with dimensional fidelity by FINCH fluorescence microscopy

Nisan Siegel,[1,2,4] Joseph Rosen,[1,2,3,5] and Gary Brooker[1,2,*]

[1]*Department of Biomedical Engineering, Johns Hopkins University, 9605 Medical Center Drive, Rockville, Maryland 20850 USA*

[2]*Microscopy Center, Johns Hopkins University Montgomery County Campus, Rockville, Maryland 20850 USA*

[3]*Department of Electrical and Computer Engineering, Ben-Gurion University of the Negev, P.O. Box 653, Beer-Sheva 84105, Israel*

[4]*nnsiegel@jhu.edu*

[5]*rosen@ee.bgu.ac.il*

**gbrooker@jhu.edu*

Abstract: Fresnel Incoherent Correlation Holography (FINCH) can faithfully reproduce objects above and below the optical plane of focus. However, as in optical imaging, the transverse magnification and optimal reconstruction depth changes based on the longitudinal distance of objects from the focal plane of the input lens with the exception that objects above and below the focal plane are in focus with FINCH and out of focus by standard optical imaging. We have analyzed these effects both theoretically and experimentally for two configurations of a FINCH fluorescence microscopy system. This information has been used to reconstruct a test planar object placed above or below the optical plane of focus with high dimensional and image fidelity. Because FINCH is inherently a super-resolving system, this advance makes it possible to create super-resolved 3D images from FINCH holograms.

OCIS codes: (090.1760) Computer holography; (090.1970) Diffractive optics; (090.1995) Digital holography; (090.2880) Holographic interferometry; (100.6890) Three-dimensional image processing; (110.0180) Microscopy; (110.6880) Three-dimensional image acquisition; (180.2520) Fluorescence microscopy; (180.6900) Three-dimensional microscopy; (260.2510) Fluorescence.

References and links

1. J. Rosen and G. Brooker, "Digital spatially incoherent Fresnel holography," Opt. Lett. **32**(8), 912–914 (2007).
2. B. Katz and J. Rosen, "Could SAFE concept be applied for designing a new synthetic aperture telescope?" Opt. Express **19**(6), 4924–4936 (2011).
3. M. K. Kim, "Adaptive optics by incoherent digital holography," Opt. Lett. **37**(13), 2694–2696 (2012).
4. J. Rosen and G. Brooker, "Non-scanning motionless fluorescence three-dimensional holographic microscopy," Nat. Photonics **2**(3), 190–195 (2008).
5. G. Brooker, N. Siegel, V. Wang, and J. Rosen, "Optimal resolution in Fresnel incoherent correlation holographic fluorescence microscopy," Opt. Express **19**(6), 5047–5062 (2011).
6. J. Rosen, N. Siegel, and G. Brooker, "Theoretical and experimental demonstration of resolution beyond the Rayleigh limit by FINCH fluorescence microscopic imaging," Opt. Express **19**(27), 26249–26268 (2011).
7. P. Bouchal, J. Kapitán, R. Chmelík, and Z. Bouchal, "Point spread function and two-point resolution in Fresnel incoherent correlation holography," Opt. Express **19**(16), 15603–15620 (2011).
8. X. Lai, Y. Zhao, X. Lv, Z. Zhou, and S. Zeng, "Fluorescence holography with improved signal-to-noise ratio by near image plane recording," Opt. Lett. **37**(13), 2445–2447 (2012).
9. B. Katz, J. Rosen, R. Kelner, and G. Brooker, "Enhanced resolution and throughput of Fresnel incoherent correlation holography (FINCH) using dual diffractive lenses on a spatial light modulator (SLM)," Opt. Express **20**(8), 9109–9121 (2012).
10. I. Yamaguchi and T. Zhang, "Phase-shifting digital holography," Opt. Lett. **22**(16), 1268–1270 (1997).

#172223 - $15.00 USD Received 9 Jul 2012; revised 2 Aug 2012; accepted 3 Aug 2012; published 14 Aug 2012

1. Introduction

The study of holography for use in collecting and manipulating three-dimensional (3D) optical information has increased rapidly in recent years as holography can gather and store large amounts of information faster than can be done with traditional two-dimensional imaging methods. An important property of holography is the collection of all of the three-dimensional optical data from objects in a 3D field with few or a single exposure, as opposed to the laborious standard optical methods of collecting stacks of 2D images as the sample or objective is translated with respect to the plane of focus of the measurement optics. In standard holography this is done by using the reflected or transmitted light from a coherent source propagating through the object and creating an interferogram with the unperturbed source, a process that generally requires a coherent source as well as the precise alignment of two laser beams. Fresnel Incoherent Correlation Holography (FINCH) [1] is a hybrid technique that has recently been introduced and which offers significant promise for recording three-dimensional information from incoherent sources such as fluorescent objects. In FINCH, the hologram is created from incoherent summation of interferences between two waves originating from each point source in an incoherently emitting object, using a single beam geometry. The key advantage of FINCH is that the object itself serves as the light source, enabling 3D imaging from any object, either by reflection or emission of light such as fluorescence. Thus a coherent laser light source and the associated precise alignment of a reference and sample beam concomitant with classical holography are not needed. The FINCH technique can be readily adapted to any standard optical imaging technique with relatively little alteration. FINCH has been theoretically investigated for its possible application to telescope optics [2,3] and more extensively studied in its application to microscopy [4–8]. While the initial report applying FINCH to microscopy demonstrated that the method could resolve a sample in three dimensions [4], subsequent studies concentrated on developing a theoretical understanding of the method and configurations to improve resolution on a single plane. We recently demonstrated that FINCH microscopy is inherently super-resolving in the lateral dimensions in comparison to conventional microscope imaging using the same optics [6]. In other optical imaging experiments [9] a more efficient FINCH configuration was demonstrated, using two closely spaced focal length lens patterns displayed on a spatial light modulator (SLM).

Because FINCH is inherently a 3D method, there is the possibility of gathering the full 3D image of an object in a few exposures at higher resolution than is possible by standard optical methods. In order to fully exploit the abilities of FINCH microscopy, it is necessary to understand what the effects are of placement of the object at positions other than at the focal plane of the objective. To date, the analysis of FINCH has been done most thoroughly for objects at the focus of the microscope objective (see Fig. 1(a)). The displacement of the object away from the focal plane of the objective, or an object with significant depth, will result in the alteration of the light cones used to create the FINCH hologram (see Fig. 1(b) and 1(c)), which will in turn affect the final reconstructed images. In this paper we theoretically and experimentally demonstrate the super-resolving performance of FINCH in three dimensions and investigate the resolving characteristics of FINCH imaging at planes above and below the objective lens plane of focus. In these studies we compare the two methods of FINCH fluorescence microscope imaging mentioned above, in which the emitted plane wave from an infinity corrected microscope objective (collimating lens) is separated with a phase only SLM into either a plane wave and one focused beam (Configuration 1) [1–7], or into two focused beams with different focal lengths (Configuration 2) [9]. To study the performance of FINCH to resolve samples above and below the plane of focus, we positioned a single plane specimen at different positions above and below the focal plane of the objective. The analysis results in methodology to accurately generate 3D images of objects with full dimensional fidelity.

#172223 - $15.00 USD Received 9 Jul 2012; revised 2 Aug 2012; accepted 3 Aug 2012; published 14 Aug 2012

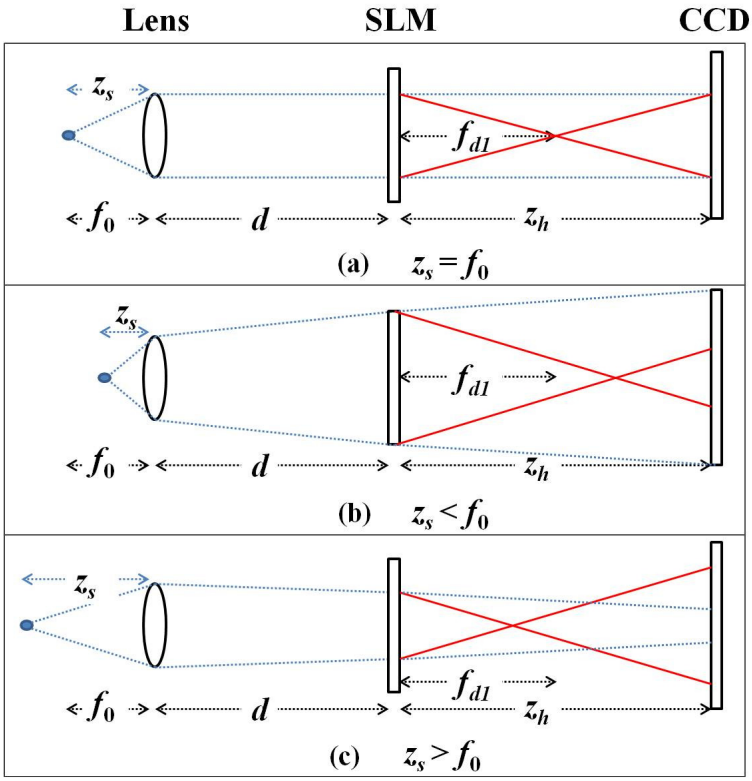

Fig. 1. Configuration 1 FINCH with the object **(a)** at the focus of the collimating lens, **(b)** above the focus of the collimating lens and **(c)** below the focus of the collimating lens. The diagram describes a static FINCH system operating on an object with significant depth above and below the focus of the collimating lens, thus f_0, d, f_{d1} and z_h remain constant over the three sub-diagrams.

2. Theoretical analysis

Following the convention in [5], and referring to the generalized diagram in Fig. 2, we consider a point source at the position $(\overline{r}_s, -z_s)$ before the input of the objective, which has the focal distance f_0. After the light from the point source propagates and moves through the objective and to the SLM, it is focused by the SLM displaying the phase components of Fresnel "lens patterns" with focal lengths f_{d1} and f_{d2}, termed the "signal" and "reference" focal lengths, respectively. After further propagation by the distance z_h, it has the complex amplitude described by:

$$u_0(x_0, y_0) = \left(C_1(\overline{r}_s) L\left(\frac{-\overline{r}_s}{z_s}\right) Q\left(\frac{1}{z_s}\right) Q\left(\frac{-1}{f_0}\right) \otimes Q\left(\frac{1}{d}\right) \right) \times \left[B exp(i\theta) Q\left(\frac{-1}{f_{d1}}\right) + B' Q\left(\frac{-1}{f_{d2}}\right) \right] \otimes Q\left(\frac{1}{z_h}\right), \quad (1)$$

where $L(\overline{s}) = exp\left[i2\pi\lambda^{-1}\left(s_x x + s_y y\right)\right]$, $Q(b) = exp\left[i\pi b\lambda^{-1}\left(x^2 + y^2\right)\right]$, C_1 is a complex constant

#172223 - $15.00 USD Received 9 Jul 2012; revised 2 Aug 2012; accepted 3 Aug 2012; published 14 Aug 2012

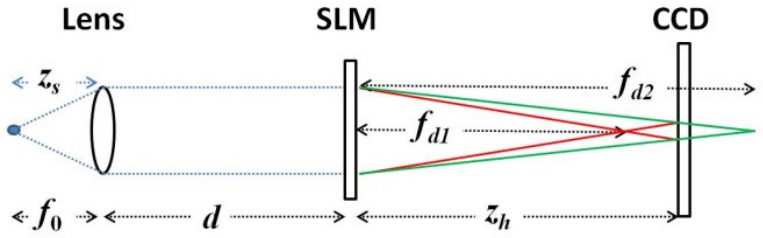

Fig. 2. A generalized diagram of FINCH showing the ability to use two spherical waves (f_{d1} and f_{d2}) to form the FINCH hologram (Configuration 2). If f_{d1} goes to $z_h/2$ and f_{d2} goes to infinity (the plane wave in Fig. 1), the system is operating with one plane wave and one spherical wave (Configuration 1).

related to the complex amplitude of the point source, the $\otimes$ symbol denotes a two-dimensional convolution, d is the distance between the objective and the SLM, B and B' are constants controlling the contribution of each lens to the hologram, θ is the constant phase factor applied to the lens pattern on the SLM to be used in the elimination of the bias term and twin image, and z_h is the distance between the SLM and the camera. In Eq. (1) we do not explicitly include the vector notation necessary to account for the polarizers used for interferometric mixing of the spherical waves [5], or a term that bounds the physical dimensions of the recorded hologram by the limiting physical aperture in the system [6].

After squaring the complex amplitude magnitude and evaluating Eq. (1), we obtain the following general expression for the intensity of the recorded point source hologram at the camera plane, which is the point spread function (PSF) for hologram formation in FINCH:

$$\begin{aligned} I_p(x,y) = C_2 + C_3(\overline{r}_s)L\left(\frac{\overline{r}_r}{z_r}\right)Q\left(\frac{1}{z_r}\right)\exp(i\theta) \\ + C_3^*(\overline{r}_s)L\left(-\frac{\overline{r}_r}{z_r}\right)Q\left(-\frac{1}{z_r}\right)\exp(-i\theta), \end{aligned} \tag{2}$$

in which C_2 and C_3 are complex constants related to the intensity of the point source, with the asterisk denoting the complex conjugate, and $\overline{r}_r$ and z_r are the transverse coordinates and the reconstruction distance of the image of the point source, respectively.

2.1 Configuration 1 - FINCH with one plane wave and one spherical wave

To review the simplest case that has been the generally considered example, we consider a hologram formed from the interference of one spherical wave with one plane wave as in Fig. 1 (referring to Fig. 2, f_{d1} is responsible for the spherical wave and the plane wave in Fig. 1 is created when $f_{d2} \to \infty$). In this case z_r and the transverse magnification M_T are given by:

$$z_r = \begin{cases} \pm(f_{d1} - z_h), & \text{for } z_s = f_0 \ \cap \ f_{d2} \to \infty \\ \pm\left(\dfrac{(f_1 + z_h)(f_e + d + z_h)}{f_1 - f_e - d}\right), & \text{for } z_s \neq f_0 \ \cap \ f_{d2} \to \infty \end{cases} \tag{3}$$

and

#172223 - $15.00 USD Received 9 Jul 2012; revised 2 Aug 2012; accepted 3 Aug 2012; published 14 Aug 2012

$$M_T = \left|\frac{\partial x_r}{\partial x_s}\right| = \begin{cases} \dfrac{z_h}{f_0}, & \text{for } z_s = f_0 \ \bigcap f_{d2} \to \infty \\ \dfrac{f_e z_h}{z_s (f_e + d)}, & \text{for } z_s \neq f_0 \ \bigcap f_{d2} \to \infty \end{cases} \tag{4}$$

where

$$f_1 = \frac{f_{d1}(f_e + d)}{f_{d1} - (f_e + d)}, \qquad \text{and} \qquad f_e = \frac{z_s f_0}{(f_0 - z_s)},$$

and the ± signs in Eq. (3) indicate that the final images may be reconstructed from either the real or the virtual image, depending on which is isolated by the phase-shift procedure [10] described below.

As Eq. (2) is the PSF of the FINCH hologram formation process, the hologram H_i of a real object is obtained as an integral of $I_P(x,y)$ over all of the object space $g(x_s,y_s,z_s)$. Typically three holograms with values of θ equally spaced by $2\pi/3$ are recorded and then superposed using the following equation to eliminate the bias term and either the real or virtual image from the reconstruction [1,10]:

$$\begin{aligned} H_F(x,y) = \quad & H_1(x,y)\left[exp\left(\pm i\theta_3\right) - exp\left(\pm i\theta_2\right)\right] \\ & + H_2(x,y)\left[exp\left(\pm i\theta_1\right) - exp\left(\pm i\theta_3\right)\right] \\ & + H_3(x,y)\left[exp\left(\pm i\theta_2\right) - exp\left(\pm i\theta_1\right)\right]. \end{aligned} \tag{5}$$

To reconstruct the image $s(x,y,z_{rec})$, the final complex valued hologram H_F is then processed computationally by Fresnel propagation:

$$s(x,y,z_{rec}) = H_F(x,y) \otimes \exp\left[\frac{i\pi}{\lambda z_{rec}}(x^2 + y^2)\right], \tag{6}$$

where z_{rec} is a parameter used to reconstruct the light field at an arbitrary distance; when $z_{rec} = z_r$ the image is in focus.

2.2 Configuration 2 - FINCH with two spherical waves

Recently it has been suggested [6] and shown [9] that the use of two spherical waves with different curvatures can be used to create more efficient FINCH holograms. This configuration, shown in Fig. 2, can provide equivalent resolution in the hologram to the method with one plane and one spherical wave, and offers the possibility of moving the camera closer to the SLM for greater light efficiency without adversely affecting the resolution in the reconstructed image. In [6] it was shown that the two spherical waves were required to overlap perfectly at the hologram recording plane in order to maintain the maximum resolution obtained with the plane wave/spherical wave method, while in [9] various methods of mixing lens patterns on the SLM were attempted, with the conclusion that a random pixel distribution of each lens pattern was the best method for displaying two lens patterns on a single SLM. Earlier work considered only objects at the focus of the objective; however in order to study 3D objects it is necessary to understand the dependence of z_r on z_s, a dependence which is reported here in the second part of Eq. (7):

#172223 - $15.00 USD Received 9 Jul 2012; revised 2 Aug 2012; accepted 3 Aug 2012; published 14 Aug 2012

$$z_r = \begin{cases} \pm\dfrac{(z_h - f_{d1})(z_h - f_{d2})}{f_{d1} - f_{d2}}, & \text{for } z_s = f_0 \ \cap f_{d2} \neq \infty \\ \pm\left(\dfrac{z_{f1} z_{f2}}{z_d^2 (f_{d1} - f_{d2})}\right), & \text{for } z_s \neq f_0 \ \cap f_{d2} \neq \infty \end{cases} \tag{7}$$

with

$$z_{fn} = z_h z_d - f_{dn}(z_d + z_h) \quad \text{and} \quad z_d = \frac{z_s(f_0 - d) + f_0 d}{f_0 - z_s}.$$

The M_T of FINCH with two spherical waves is the same as that with one plane and one spherical wave, shown in Eq. (4), so that the effects of object depth must still be accounted for when reconstructing FINCH holograms taken with the double lens pattern method.

3. Experimental methods

The fluorescence microscope apparatus and FINCH holography setup used in these experiments has been previously described [6]. Briefly, an upright microscope was modified so that in place of the tube lens there was a phase-only SLM (Holoeye 1080P, 1920 × 1080 pixels) centered over the objective and positioned at a 45° angle to the beam path from the output of the infinity objective. The SLM displays quadratic phase lens patterns of the form

$$exp\left[-\frac{i\pi}{\lambda a}\left(x^2 + y^2\right) + i\theta\right], \tag{8}$$

with focal length $f_{dn} = a$, where λ is the central wavelength of light passed by the emission filter to the SLM. The angle θ is a constant phase factor that can be added to the phase to enable the superposition of several holograms to eliminate bias and the twin-image term. The parameter a used to calculate the lens pattern was corrected for SLM characteristics such as format, pixel dimension and substrate curvature as described in [5], and has additional corrections applied due to the 45° incidence angle of the light from the objective. The sample was a USAF negative test pattern slide (Max Levy Autograph) displaying the smallest features of the test pattern (group 9 which had reduced visibility by standard microscopic imaging with the 20x 0.75 NA objective), mounted over a fluorescent plastic slide.

Two configurations of FINCH were used, including one utilizing polarization to obtain interference between a plane wave and a spherical wave (as in [5] and [6]) and one using two lens patterns to obtain interference between two spherical waves (as in [9]). As shown in Fig. 3(a), for Configuration 1, with one plane wave and one spherical wave, light propagating from the objective passed through a polarizer with t-axis 45° to the SLM polarization axis, then onto the SLM, which passed half the light unchanged and which focused half the light by the focal length f_{d1}. The light then propagated through another polarizer at the same angle as the first, allowing the projections of both the focused and unfocused light along the polarizer axis to interfere with each other and create a hologram. For Configuration 2, with two lens patterns distributed randomly over the SLM, only one polarizer was used as shown in Fig. 3(b), which was placed before the SLM and aligned to be polarized parallel to the SLM. The two lens patterns were selected to provide matching sizes of the unfocused light cones at the camera plane, with $f_{d1} < z_h$ and $f_{d2} > z_h$. In both configurations, the hologram was recorded at the distance z_h from the SLM by a CCD camera (QImaging Retiga 4000R, cooled, 2048 × 2048 pixels).

#172223 - $15.00 USD Received 9 Jul 2012; revised 2 Aug 2012; accepted 3 Aug 2012; published 14 Aug 2012

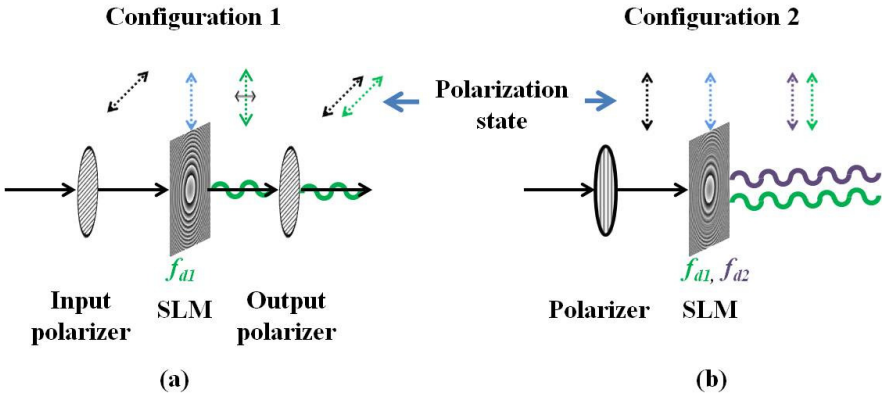

Fig. 3. Schematic representation of polarizations of interfering beams in two FINCH configurations. **(a)** Configuration 1, with one spherical wave and one plane wave. Only one lens pattern is displayed on the SLM; two polarizers are necessary to split the incoming beam and recombine it to achieve interference while maintaining complete coincidence of both waves. **(b)** Configuration 2, with two spherical waves. Two lens patterns are displayed on randomly selected pixels on the SLM, focusing the waves to different focal lengths. Only one polarizer is required to align the incoming waves polarization with the SLM.

Three holograms with phase factors θ differing by $2\pi/3$ were recorded and superposed to create H_F, the bias-eliminated complex-valued hologram.

The sequence of holograms taken with Configuration 1 were to confirm the relationships of z_{rec} and M_T to distance away from the focus of the objective, given static values for all other parameters. A Nikon Plan Apo 20x, 0.75 NA (air) infinity-corrected objective was used for these experiments. Similar results (not shown) were obtained using other lenses including an Olympus UApo/340 20x 0.75 NA (air) infinity-corrected objective, and an achromatic doublet lens with 30 mm focal length (Thorlabs part #AC254-030-A-ML). The excitation filter and dichroic mirror in the microscope were Semrock Cy3, and the emission filter was a Thorlabs interference filter passing 570 $\pm$5 nm light. The SLM displayed a "lens pattern" calculated for a 570 nm central wavelength and a 767 mm f_{d1}, with the CCD positioned at a z_h of 1380 mm from the SLM. This proportion of z_h:f_{d1} is in the range reported in [6] resulting in the best focused reconstructed images for this SLM with these experimental parameters. The axial position z_s of the object, the single plane USAF test pattern, was adjusted over a range of 30 microns above to 30 microns below the focal plane of the objective. FINCH holograms were recorded for each position without changing any of the SLM or camera parameters. For each z_s position of the object, the complex-valued hologram was processed by the Fresnel propagation method using Eq. (6) over a range of z_{rec} values, and the best focused reconstructed image for each hologram was selected. Linear FINCH reconstructions were used [6]. The z_{rec} values of the best focused image from each hologram were recorded, as were the widths (in pixels) of the vertical and horizontal features in Element 1 of Group 8 for determination of the lateral magnification.

A similar series of experiments was done with Configuration 2, with several differences. The lens patterns were calculated for a central wavelength of 520 nm, the excitation filter and dichroic mirror were Semrock GFP, the emission filter was a Thorlabs interference filter with a central wavelength of 520 $\pm$5 nm, and the z_h distance was 600 mm. Experiments were done only with the Nikon 20x objective, and holograms were taken for z_s values between 10 microns above and 10 microns below the focal plane of the objective. Four pairs of lens patterns with differing focal length spacing factors between the two lens patterns s_{fac} = 0.05, 0.10, 0.15, 0.20 were used, where

$$s_{fac} = \left(z_h / f_{d1}\right) - 1 = 1 - \left(z_h / f_{d2}\right). \quad (9)$$

#172223 - $15.00 USD Received 9 Jul 2012; revised 2 Aug 2012; accepted 3 Aug 2012; published 14 Aug 2012

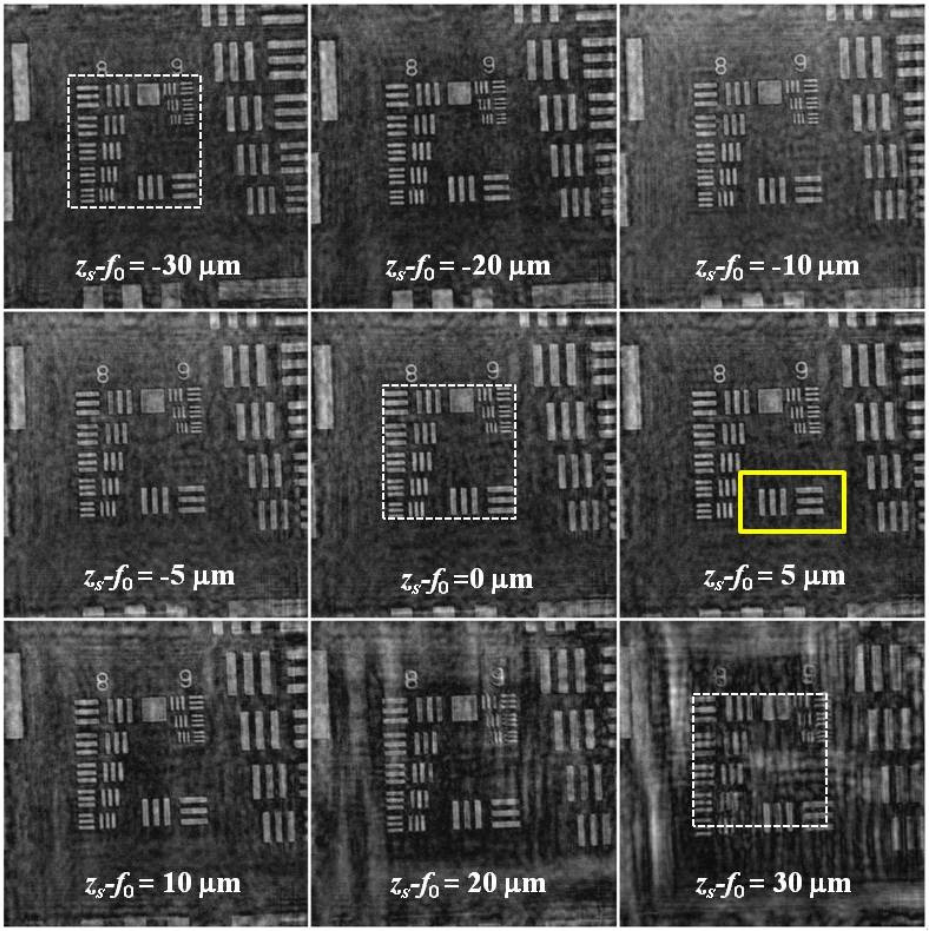

Fig. 4. The best focused reconstructed Configuration 1 FINCH (linear reconstruction) images from selected values of z_s-f_0. The yellow outline shows Group 8, Element 1, which were the features measured to determine the magnification in the series of holograms taken with the Nikon objective. The dashed squares on the reconstructed images show that in reference to images calculated from the hologram captured at the focus of the objective (center image), the image above (top left) and below (bottom right) the optical plane of focus from the holographic reconstructions were either smaller or larger.

4. Results and discussion

4.1 Configuration 1

A selection of the best reconstructed images from the holograms taken with the Nikon objective is shown in Fig. 4. Reconstructed images from holograms taken with the other objective lenses were of similar quality and are not shown here. As the object was brought down from z_s-f_0 = −30 µm (above the focal plane of the objective), the reconstructed images were increasingly magnified, a process that continued through the focus of the objective (z_s-f_0 = 0 µm) and until the sample was brought to below the focal plane of the objective to z_s-f_0 = 30 µm. For holograms taken with z_s-f_0 > 15 µm there was significant degradation of the reconstructed images; however for holograms taken over the range of z_s-f_0 = −30 to 15 µm the reconstructed images are all relatively equal in quality though they differ significantly in

#172223 - $15.00 USD Received 9 Jul 2012; revised 2 Aug 2012; accepted 3 Aug 2012; published 14 Aug 2012

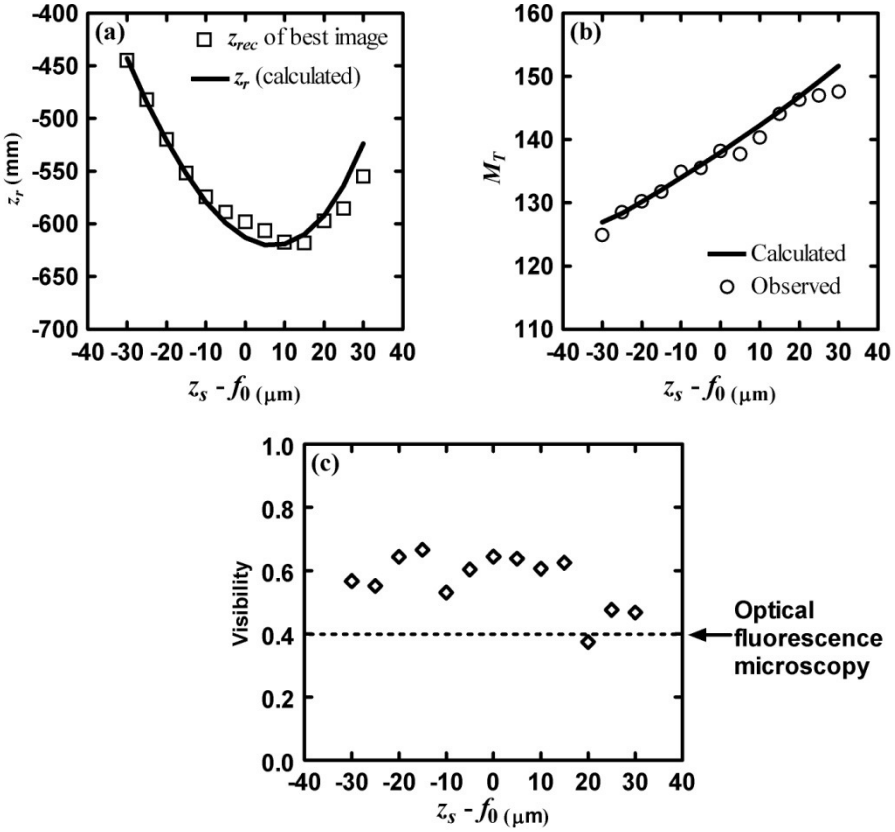

Fig. 5. Performance of the FINCH microscope with Configuration 1, using the Nikon 20x objective. **(a)** The reconstruction depth z_{rec} of the best focused reconstructed image from the experimental holograms plotted as a function of z_s-f_0, the distance above or below the focus of the objective, plotted against a theoretical curve of z_r based on Eq. (3) and using our experimental parameters as discussed in the text. **(b)** The transverse magnification M_T of Element 1 of Group 8 of the USAF pattern, measured vertically and horizontally in the best reconstructed FINCH images and averaged, as a function of z_s-f_0. For comparison, a theoretical curve of M_T is plotted, based on Eq. (4) and using our experimental parameters as discussed in the text. **(c)** The visibilities of the horizontal Group 9 Element 3 features of the USAF pattern. The dashed line is the level of the visibility of those features in standard optical fluorescence microscopy.

magnification. The visibilities of the smallest horizontal features in the USAF pattern for standard fluorescence widefield microscopic images and images reconstructed from holograms were measured by the previously reported method [6]. The visibilities for the range of $z_s - f_0 = -30$ to 15 μm for the reconstructed images from holograms were found to be between 0.53 and 0.67 in the linear reconstructions compared to 0.4 when the microscope was used as a traditional microscope with the properly matched and configured tube lens (see Fig. 5(c)). Since the gaps and features of the smallest USAF objects measured (775 nm) are both on the order of the Abbe diffraction limit for this objective (380 nm), the width of the PSF has a strong effect on visibility and therefore the visibility of these features serves as a good measure of the resolving power of the system. Thus the FINCH method maintains an advantage over widefield fluorescence microscopy even for images taken at significant distances away from the focus of the objective lens.

The experimental z_r and M_T data are plotted in Fig. 5 alongside the theoretical values for the optimal z_r and M_T that were calculated using Eqs. (3) and (4). For convenience we identify

#172223 - $15.00 USD Received 9 Jul 2012; revised 2 Aug 2012; accepted 3 Aug 2012; published 14 Aug 2012

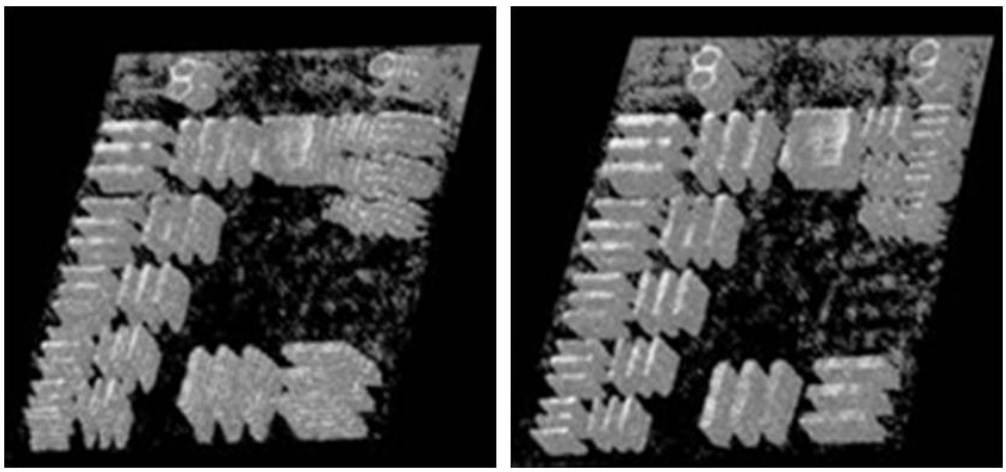

Fig. 6. 3D views (by direct volume rendering) of stacks of reconstructed Configuration 1 FINCH images of the USAF pattern taken at z_s ranging from 30 μm above f_0 to f_0.The left image is the 3D view of images as calculated by Eq. (6), without any size adjustments. The right image is the 3D view of reconstructed images that were resampled based on the ratio of M_T:M_{T0} as discussed in the text, and registered to lie directly over each other creating a clear well resolved 3D image. Notice that without correction, the smallest features in group 9 patterns are severely distorted, limiting resolution of 3D images.

the z_r and M_T at z_s-f_0 = 0 μm as z_{r0} and M_{T0}. For the calculated values, the Nikon compound objective lens was treated as a thin lens with $f_0 = f_{tube}/Mag$, where f_{tube} was the focal length of the matching tube lens (200 mm) and Mag is the rated magnification factor of the objective lens when used in a standard microscope configuration. The remainder of the length of the objective was added to d, the distance between the collimating lens and the SLM. Thus for both configurations, using the Nikon 20x objective, d = 320 mm and f_0 = 10 mm. Since z_r as a function of z_s-f_0 reaches a minimum and then begins to increase again, in order to obtain reconstructions which faithfully represent a 3D object, it is important that the object be fully on one side or the other of the z_r minimum. If the object spans the z_r minimum in both directions, object points from planes above and below the plane of minimum z_r will reconstruct in the same image plane, making it difficult to determine whether reconstructed image points represent objects from above or below the point of minimum z_r. In practice this problem can be avoided by obtaining holograms when objects are only above or below the minimum z_r, which is usually near the optical plane of focus.

Another important feature of FINCH can be seen in Fig. 4; the size of the reconstructed image changes significantly when the object is moved over a range of z_s that could easily correspond to a "real-world" application. For such "real-world" applications, though, it would be preferable if the M_T of each reconstructed image was the same and the image space was telecentric. It has been shown [7] that telecentricity in FINCH images can be obtained by setting $d = f_0$. However, with most high NA compound microscope objectives this is impossible, as f_0 is usually significantly smaller than the physical length of the objective. Thus we resample all the images to match the size of the image in the stack that has the highest magnification. This choice of reference image ensures that no data is lost during resampling. Shown in Fig. 6 are the top and side views of 3D projections of stacks of the USAF pattern taken at positions ranging from 30 microns above objective focus to the objective focus. One set is presented without processing while the other has been resampled to ensure that the resampled images were aligned properly in reconstruction space as the object was in object space during hologram recording. The corrected image shown in the right panel of Fig. 6 presents a view of the 3D object volume that does not display increasing size going from top to bottom, which is present in the uncorrected image and is characteristic of the perspective

#172223 - $15.00 USD Received 9 Jul 2012; revised 2 Aug 2012; accepted 3 Aug 2012; published 14 Aug 2012

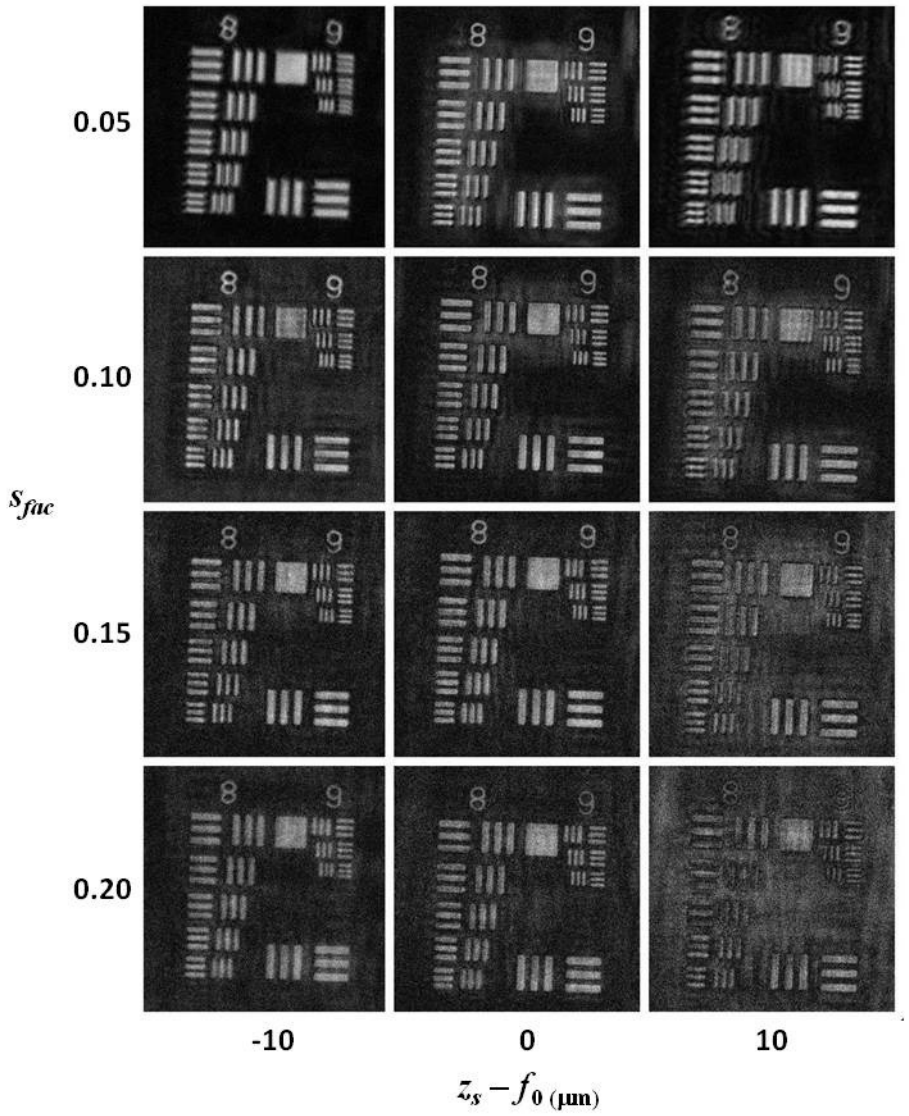

Fig. 7. Cropped sections from linear Configuration 2 FINCH reconstructions showing the smallest USAF groups. Images are from dual-lens pattern FINCH holograms taken at various locations with respect to the objective focus and with various spacings s_{fac} between the lens patterns.

effect on the FINCH process resulting from lack of telecentricity when using high power, high NA objective lenses.

4.2 Configuration 2

Four sets of lens patterns were used to record FINCH holograms of the USAF pattern using the Nikon 20x objective, in steps of two microns over a distance of 10 microns above objective focus to 10 microns below. The camera distance z_h was set at 600 mm in order to reduce the optical path difference (OPD) of this configuration [9]. Selected images at focus and 10 microns above and below focus are shown in Fig. 7.

The z_{rec} values and M_T were recorded for each reconstructed image and are shown in Fig. 8

#172223 - $15.00 USD Received 9 Jul 2012; revised 2 Aug 2012; accepted 3 Aug 2012; published 14 Aug 2012

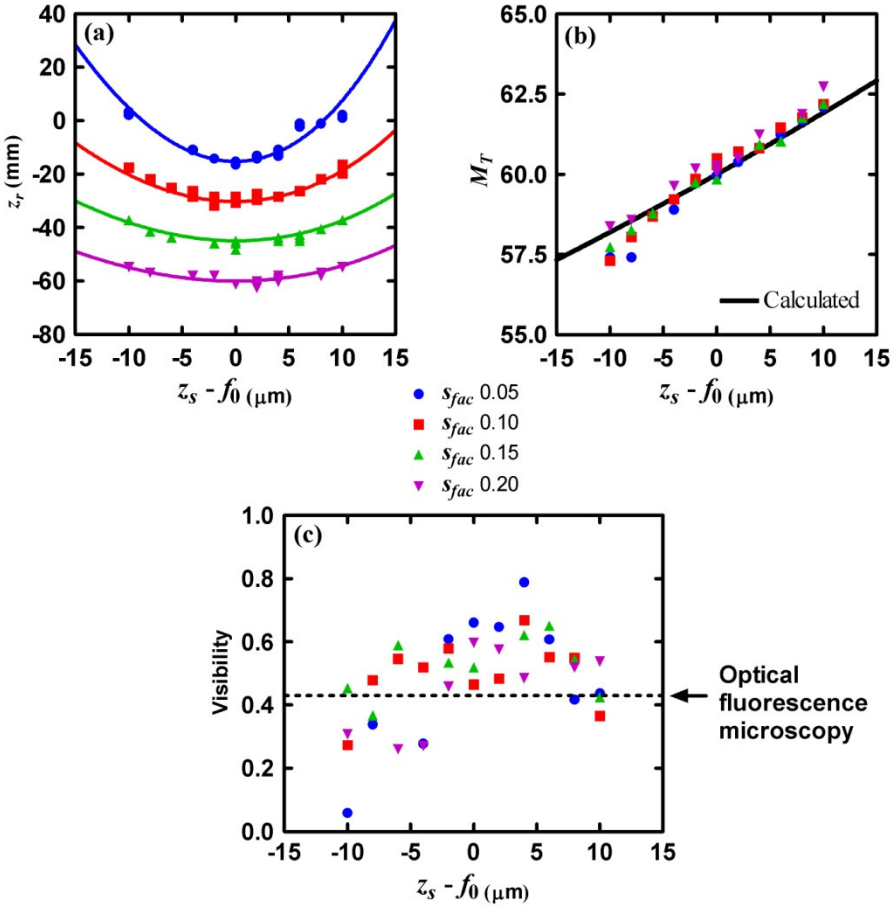

Fig. 8. FINCH microscopy with two spherical waves. **(a)** The reconstruction depth z_{rec} of the best focused reconstructed images from the experimental holograms (circles, squares, triangles) is plotted as a function of z_s-f_0 and shown against theoretical curves (solid lines) of z_r for that s_{fac} based on Eq. (7) and using our experimental parameters as discussed in the text. **(b)** The transverse magnification M_T of Element 2 of Group 6 of the USAF pattern, showing the average of the horizontal and vertical measurements, as a function of z_s-f_0. For comparison, a theoretical curve of M_T is plotted, based on Eq. (4) and using our experimental parameters as discussed in the text. **(c)** The visibilities of the horizontal Group 9 Element 3 features of the USAF pattern. The dashed line is the level of the visibility of those features in standard optical fluorescence microscopy.

plotted against theoretical curves of z_r and M_T calculated from the parameters used in the hologram recording. When more than one reconstructed image was equivalent in quality, the z_{rec} of each equivalent image was recorded. It is apparent from these experiments that the relative reduction in image quality, as measured by the visibility of the smallest features [6] shown in Fig. 8(c), when moving above or below the objective focus is more pronounced for the smaller s_{fac}, while the image background and noise that are visible in the images are greater for larger s_{fac}. The latter observation may be understood as being due to the larger OPD between the signal and reference beams, but the reason for the former observation is less obvious. However, we may consider NA_H, the NA of the hologram of an infinitesimal point, as a limiting factor on the quality of the reconstructed images. As previously shown [6,9], the minimum resolved object feature size in FINCH is inversely proportional to $NA_H \times M_T$. The visibility, then, is proportional to this factor. To calculate NA_H for objects away from the objective focal plane, we note that at the detector plane, the radius of the nth spherical wave

#172223 - $15.00 USD Received 9 Jul 2012; revised 2 Aug 2012; accepted 3 Aug 2012; published 14 Aug 2012

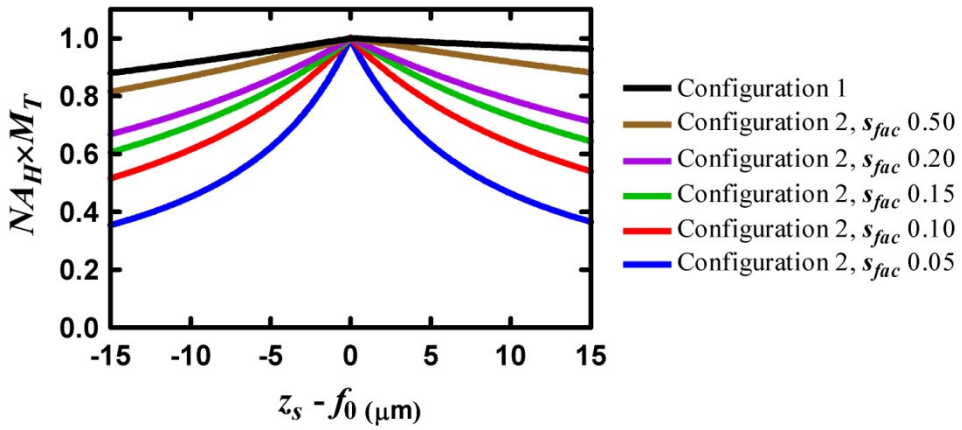

Fig. 9. $NA_H \times M_T$ as a function of z_s-f_0 for FINCH with a plane and spherical wave (Configuration 1) and two spherical waves (Configuration 2) with various spacing factors s_{fac} for two lens patterns displayed on the SLM.

coming from the objective through the SLM is given by:

$$R_n = \left| \frac{f_{dn}^{(eff)} - z_h}{f_{dn}^{(eff)}} \right| R_0, \qquad \text{with} \qquad f_{dn}^{(eff)} = \frac{f_{dn}\left(d + f_e\right)}{d - f_{dn} + f_e}, \tag{10}$$

in which R_0 is the radius of the limiting aperture in the system (in this case the SLM radius, approximated as 10 mm due to the 8.6 mm length in the short dimension and ~11 mm projection of the long dimension at 45° angle of incidence) and $f_{dn}^{(eff)}$ is the effective focal length (image distance) of the lens pattern when $z_s \neq f_0$, derived using the equation for lenses in series. When $z_s = f_0$, $f_{dn}^{(eff)} = f_{dn}$. If we consider that the radius of the hologram is bounded by the radius R_{min} of the smaller of the two spherical waves, then the NA of the point hologram originating from any plane before the objective may be written formally as $NA_H = sin(arctan(R_{min}/|z_r|))$. Figure 9 shows plots of calculated $NA_H \times M_T$ for both Configuration 1 and Configuration 2, for f_0 = 10 mm, d = 320 mm, and z_h = 600 mm, including the values of s_{fac} studied in this research. The maximum $NA_H \times M_T$ is the same for both configurations, while the $NA_H \times M_T$ curve as a function of z_s-f_0 falls off more sharply as the s_{fac} becomes smaller. This shows that in addition to the z_r and M_T effects mentioned in the previous section, the choice of configuration and s_{fac} will alter the level of background and noise as well as on the depth of field in which well-resolved images are obtained.

5. Conclusion

We have analyzed the dependence of reconstruction depth and transverse magnification on displacement of the object away from the focus of the objective lens in FINCH microscopy using two different configurations, one with one spherical and one plane wave and another with two spherical waves to form the interference pattern. We have also analyzed these dependencies and shown their implication for successful measurement of the 3D light field emitted by the object and its formation into accurate 3D images:

1. The light used to form the hologram must originate entirely from a collection of points above or below the plane defined by the minimum of the z_r curve. This plane is generally at or near the focus of the objective.

#172223 - $15.00 USD Received 9 Jul 2012; revised 2 Aug 2012; accepted 3 Aug 2012; published 14 Aug 2012

2. The reconstructed images in a stack must be resampled according to the largest magnification in the stack in order to avoid distortions in 3D rendering resulting from significant changes in M_T with change in object location.

3. Choice of FINCH configuration lens pattern focal length spacing, s_{fac} has significant effects upon reconstructed image background noise, resolution and on depth of the FINCH field, which must be accounted for when designing a FINCH system.

4. In-focus images with resolution beyond optical limits can be obtained by FINCH for objects not only at the focal plane of the microscope objective, as previously demonstrated with one of the FINCH configurations [6], but now is shown for objects above and below the focal plane of a microscope objective. This conclusion is based on data in Figs. 5(c) and 8(c) for both FINCH configurations in which one can see that the visibility, and therefore the resolution, of objects near diffraction limited size is not only better than a standard widefield microscope at the plane of focus but also along a range of ± 5-30 μm from the objective focal plane.

Acknowledgments

This work was supported by NIST ARRA Award No. 60NANB10D008 to GB, The Israel Ministry of Science and Technology (MOST) to JR and by CellOptic, Inc.

#172223 - $15.00 USD Received 9 Jul 2012; revised 2 Aug 2012; accepted 3 Aug 2012; published 14 Aug 2012